This is the accepted manuscript made available via CHORUS. The article has been published as:

Accelerator Measurements of Magnetically Induced Radio Emission from Particle Cascades with Applications to Cosmic-Ray Air Showers

K. Belov *et al.* (T-510 Collaboration)

Phys. Rev. Lett. **116**, 141103 — Published 7 April 2016

DOI: 10.1103/PhysRevLett.116.141103

Accelerator measurements of magnetically-induced radio emission from particle cascades with applications to cosmic-ray air showers

K. Belov,[1,2] K. Mulrey,[3] A. Romero-Wolf,[2] S. A. Wissel,[1,4,*] A. Zilles,[5] K. Bechtol,[6] K. Borch,[1] P. Chen,[7] J. Clem,[8] P. W. Gorham,[9] C. Hast,[10] T. Huege,[11] R. Hyneman,[1,12] K. Jobe,[10] K. Kuwatani,[1] J. Lam,[1] T. C. Liu,[7] J. Nam,[7] C. Naudet,[2] R. J. Nichol,[13] B. F. Rauch,[14] B. Rotter,[9] D. Saltzberg,[1] H. Schoorlemmer,[9] D. Seckel,[8] B. Strutt,[13] A. G. Vieregg,[6,15] and C. Williams[16]

(T-510 Collaboration)

[1] *Dept. of Physics and Astronomy, Univ. of California, Los Angeles, Los Angeles CA 90095, USA*
[2] *Jet Propulsion Laboratory, Pasadena CA 91109, USA*
[3] *Dept. of Physics and Astronomy, Univ. of Delaware, Newark DE 19716, USA*
[4] *Dept. of Physics, California Polytechnic State Univ., San Luis Obispo CA 93407, USA*
[5] *Institut für Experimentelle Kernphysik, Karlsruher Institut für Technologie, 76128 Karlsruhe, Germany*
[6] *Kavli Institute for Cosmological Physics, Univ. of Chicago, Chicago IL 60637, USA*
[7] *Dept. of Physics, Grad. Inst. of Astrophys., National Taiwan University, Taipei Taiwan*
[8] *Dept. of Physics, Univ. of Delaware, Newark DE 19716, USA*
[9] *Dept. of Physics and Astronomy, Univ. of Hawaii, Manoa HI 96822, USA*
[10] *SLAC National Accelerator Laboratory, Menlo Park CA, 94025, USA*
[11] *Institut für Kernphysik, Karlsruher Institut für Technologie, 76021 Karlsruhe, Germany*
[12] *Physics Dept., College of William & Mary, Williamsburg VA 23187, USA*
[13] *Dept. of Physics. Univ. College London, United Kingdom*
[14] *Dept. of Physics, Washington Univ. in St. Louis, St. Louis MO 63130, USA*
[15] *Dept. of Physics, Enrico Fermi Institute, Univ. of Chicago, Chicago IL 60637, USA*
[16] *Dept. of Physics, Stanford Univ., Stanford CA, 94305, USA*

(Dated: January 21, 2016)

For fifty years, cosmic-ray air showers have been detected by their radio emission. We present the first laboratory measurements that validate electrodynamics simulations used in air shower modeling. An experiment at SLAC provides a beam test of radio-frequency (RF) radiation from charged particle cascades in the presence of a magnetic field, a model system of a cosmic-ray air shower. This experiment provides a suite of controlled laboratory measurements to compare to particle-level simulations of RF emission, which are relied upon in ultra-high-energy cosmic-ray air shower detection. We compare simulations to data for intensity, linearity with magnetic field, angular distribution, polarization, and spectral content. In particular, we confirm modern predictions that the magnetically induced emission in a dielectric forms a cone that peaks at the Cherenkov angle and show that the simulations reproduce the data within systematic uncertainties.

PACS numbers: 95.55.Vj, 98.70.Sa, 29.27.-a

The highest energy cosmic rays arrive at Earth with energies in excess of 10^{20} eV. Despite decades of work meant to uncover their sources, their origin remains elusive. Observations are limited by the low flux at the end of the cosmic-ray spectrum, calling for the development of new techniques with high duty cycles, high precision, and large surface areas. One promising technique makes a measurement of the radio-frequency electric field from a cosmic-ray air shower, which is nearly linear with the energy of the primary particle.

Radio emission arises from a cascade of charges moving inside a dielectric and in the presence of magnetic field in two main ways. Askaryan radiation forms from a charge excess built up in the shower due to Compton, Bhabha, and Møller scattering and positron absorption, forming a current along the shower axis and radio frequency emission [1]. Such emission has been measured in accelerator experiments [2–6]. Geomagnetic emission forms when the Lorentz force acts on charges in the shower, generating a time-varying transverse current. The former is present even with no magnetic field, and the latter is present even without a charge asymmetry. In practice, experiments detect the sum of these two effects.

Several experiments have detected radio emission from cosmic-ray air showers [7–22]. To progress from event detection to measurement of a differential energy flux, one needs to know the intensity and angular distribution of the radio emission and its frequency dependence. To date, predictions of these parameters have relied on simulations and measurements of air showers themselves, which can be subject to uncertainties in geometry and hadronic interactions in addition to uncertainties related to the radio emission. In contrast, this work provides a direct laboratory benchmark for the simulations of the radio emission using particle showers with well-known cascade physics that develop in a precisely known target and geometry.

Our particle showers developed in a dense plastic instead of rarefied atmosphere. Increasing the density, ρ, decreases the shower length, thereby reducing the total

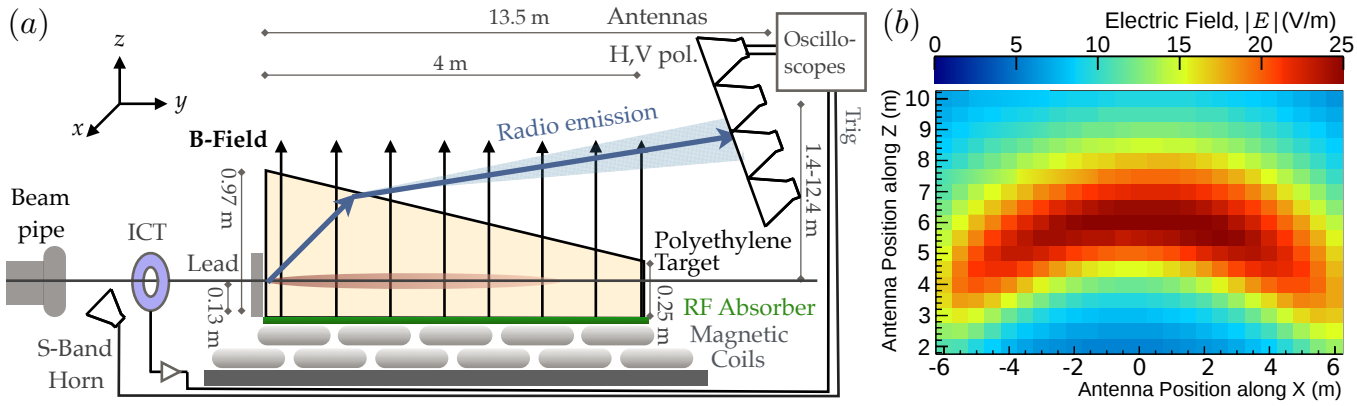

FIG. 1. (a) Schematic of the experiment, not to scale. (b) Simulated (Endpoints) electric field, $|E|$, in the x-z plane with full magnetic field, 131 pC, and 4.35 GeV.

amplitude of both radiations integrated over the whole shower. The total Askaryan radiation scales with the shower length as $1/\rho$, weighted by the charge asymmetry. Because the magnetic radiation from a given position in the shower is proportional to the transverse drift velocity of electrons and positrons, the magnetic radiation per unit track length scales with the magnetic field B and the scattering length [23], or B/ρ. The total magnetic radiation for the entire shower scales as B/ρ^2, meaning that the expected ratio of magnetic to Askaryan radiations scales as B/ρ. So, in order to achieve the same relative emission amplitude found in air showers, we increased the magnetic field from the terrestrial 0.5 Gauss to 1000 Gauss, commensurate with an increase in density from air to plastic.

Two formalisms, ZHS [24] and Endpoints [25], are at the heart of recent simulations of radio emission, ZHAireS [26] and CoREAS [27], respectively. They both treat each shower particle track as an independent radiator, summing up the emission from all tracks in the cascade to obtain the signal that would be received by an observer. The ZHS technique has been adapted to the time-domain [28] and calculates the vector potential of each particle track. The Endpoints formalism sums the radiation due to the acceleration between discrete segments of the particles' trajectories [25]. Both formalisms are compared to the accelerator data in this paper.

The T-510 experiment, shown schematically in Fig. 1a, took place at the End Station Test Beam (ESTB) in End Station A (ESA) at SLAC. Bunches of electrons with energy 4.35 or 4.55 GeV passed through 2.3 radiation lengths of lead pre-shower and entered a plastic target, generating compact showers with total energy equivalent to a $\sim 4 \times 10^{18}$ eV primary cosmic ray.

The target was formed from 5.08 cm $\times$ 10.16 cm $\times$ 30.48 cm bricks of high-density polyethylene (HDPE) with density 0.97 g/cm^3. Being 4 m long, 0.96 m tall, and 0.60 m wide, it contained the majority of the particle shower. The beam was 0.13 m above the bottom of the target. The bricks on the top surface were machined to a 9.8 degree angle below horizontal to avoid total internal reflection. The index of refraction of HDPE is 1.53, resulting in a refracted Cherenkov angle of 28° from the horizontal (49° before refraction). Rays emanating from the target at the refracted Cherenkov angle intersected the antenna plane at 6.5 m above the position of the beam. The target floor was lined with an RF absorbing blanket. Several pieces of ANW-79 absorber were placed at both sides of the target and at the exit surface of the target.

Fifteen water-cooled coils placed under the target were used to create a vertical magnetic field of up to $\pm$970 G. This was achieved by supplying sets of five coils in series up to 2400 A direct current with reversible polarity. The coils were aligned along the beam axis on a 10.16 cm thick steel plate and were staggered in two rows in order to create a more uniform magnetic field. The vertical magnetic field measured at the beam height and maximum current had a RMS variation of 72 G. The magnetic field was strong enough to bring the expected intensity from the magnetic effect to the same order of magnitude as that expected from the Askaryan effect.

Four dual-polarization, quad-ridged horn antennas used in the ANITA experiment [29] recorded the electric fields generated in the particle shower. An overhead crane allowed for the movement of the antenna array to sample the electric field at many positions. The antenna array was placed at the far wall of ESA, 13.5 m from the entrance of the beam to the target. It was tilted at 19.6° to better align the expected radiation with the boresight of the antennas. The antenna array covered vertical distances between 1.4 m and 12.4 m, corresponding to angles between 40° and 55° with respect to the beam line at the beam entry point, which, due to the lead pre-shower, is close to shower maximum.

The antennas used are sensitive to the 200-1200 MHz

band. The comparable frequency range in air showers is lower, because it is inversely proportional to both the Molière radius and $\sin\theta$, where θ is the observation angle. The Moilère radius scales as $1/\rho$ and $\sin\theta$ scales as $\sqrt{\rho}$ to first order. Taken together, we expect that the frequencies scale as $\sqrt{\rho}$. The T-510 bandwidth translates to approximately 10-60 MHz in air showers, comparable to the bandwidth of ground-based air shower experiments.

Signals from each antenna ran through 15.24 m of LMR240 coaxial cable and a low-pass filter with a 3 dB point of 1250 MHz to avoid aliasing during data acquisition. Time-series voltages from the horns were collected on 2.0 GHz, 5 GSa/s oscilloscopes. A global trigger was provided by the broadband transition radiation produced by the beam exiting the beam pipe, collected in an S-band horn antenna. Events were recorded at 1 Hz.

The beam charge was measured using an integrating charge transformer situated between the beam pipe and the target. The mean bunch charge was 131 pC, with a shot-to-shot standard deviation of 3 pC. Measurements of the bunch charge at several positions indicate a 2% systematic uncertainty.

Particle showers were simulated with GEANT4, using the measured magnetic field. Five thousand primary electrons were injected, and the results were scaled to 131 pC. The radio emission was then simulated following the ZHS and Endpoints formalisms. In calculating the radiation from each track we included refraction, Fresnel coefficients, and demagnification effects [30] at the surface of the target.

The simulation, shown on the right in Fig. 1b, demonstrates that the expected radiation forms a ring when projected onto a two-dimensional plane 13.5 m from the entrance to the target, peaking at about 6.5 m above the shower axis. The electric field strength, $|E|$, map shows the superposition of magnetic and Askaryan components. Since the magnetic field is vertical at the shower, the former is horizontally polarized, whereas the polarization of the Askaryan contribution points radially from the shower axis. The interference between the two produces the left-right asymmetry shown in the figure. Refraction at the target surface makes the ring elliptical rather than circular. The ring is cut off on both sides due to the finite target. The simulation is done using ray optics. The top of the target acts as a diffractive slit, with a Fresnel zone of about 60 cm at 300 MHz, which is smaller than the length of the target. The target width ($\pm$30 cm) corresponds to a phase lag of about 30°, and so we expect the simulation to modestly overestimate $|E|$ at low frequency. Reflections were not included in Fig. 1b, but are discussed below. Effects due to transition radiation were estimated and found to be two orders of magnitude below the Askaryan radiation.

By design, at our antenna locations, the two types of radiation separate into orthogonal polarizations. The magnetic is horizontally polarized, while the Askaryan is vertical. However, in real antennas, the vertical signal leaks into the horizontally polarized channel at about the 25% level in amplitude (about -12 dB in power). We eliminate this leakage in the horizontal polarization by construction in using the difference between field-up, $V_{B_+}(t)$, and field-down, $V_{B_-}(t)$, data, namely $V(t) = \frac{1}{2}(V_{B_+}(t) - V_{B_-}(t))$. Each waveform is also scaled by the beam bunch charge to 131 pC. When this construction is applied to the vertically polarized signal, we see only noise, as expected. The resulting single-acquisition waveform from the horizontal polarization at maximum magnetic field strength is shown in Fig. 2a. Fig. 2b shows the power spectral density normalized by the sampling interval 200 ps/point for the data and 100 ps/point for the simulations.

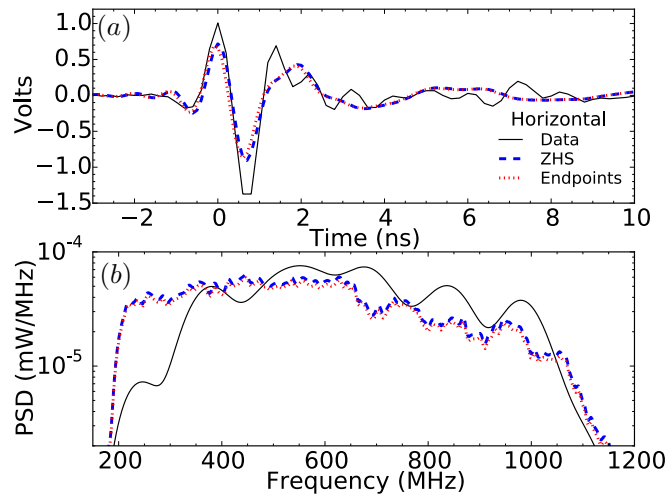

FIG. 2. (a) Simulated and measured voltages 6.52 m above the beam in the horizontal polarization channel at full magnetic field. (b) Corresponding power spectral densities.

For comparison with the data, the simulated electric fields were convolved with the measured antenna effective heights [29] and response due to the cables and filters used in the system. The convolution was performed in the frequency domain following standard techniques [31]. The predicted values in Fig. 2 from the ZHS and Endpoints formalisms agree to within 3% in peak amplitude and 7% in integrated power. The dominant features in the time-domain waveform arise from antenna response and filters, which the two simulations have in common. The shape of the simulated waveforms reproduces the data well, giving us confidence in the experimental modeling. The absolute scale is discussed below.

Internal reflections from the bottom of the target interfered with the signal transmitted through the top surface of the target, which is apparent in the modulation of the power spectral density in Fig. 2b. A low amplitude reflection with two internal bounces arrived at the antenna $\sim$ 7 ns after the main pulse, and was responsible for the $\Delta f \simeq$ 150 MHz frequency beat in Fig. 2b.

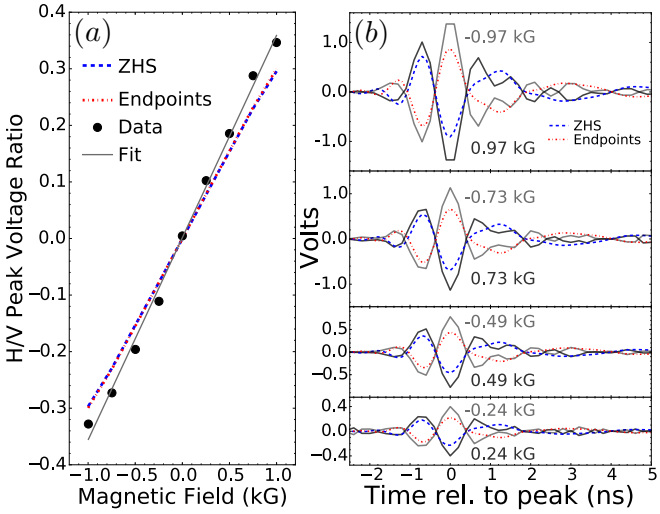

FIG. 3. (a) Horizontally polarized signal normalized by vertical showing the expected linear behavior vs. magnetic field. (b) The oscilloscope traces (solid) show the polarity flip. Models (dashed) are shown for opposite polarities.

More important is the radiation that reflected only once off the bottom of the target. Assuming that the absorber has a higher index of refraction than the HDPE, that reflection arrived at the antenna $\sim$ 1 ns after the direct pulse, but with inverted polarity. Adding a time delayed equal amplitude reflection to the direct pulse for a particular antenna varies the simulated peak time-domain amplitude by a factor of up to 1.38 for horizontal polarization and 1.43 for vertical polarization. Thus, averaged over 300-1200 MHz, the uncertainty in the models due to reflections is of order 40% for both polarizations. We exclude the 200-300 MHz band in the data and simulation comparisons due to uncertainties related to diffraction and in the antenna response at low frequencies [29]. For the horizontal polarization shown in Fig. 2a, the time-domain peaks of the data exceed the simulations by 35%, commensurate with the systematic uncertainty.

Fig. 3 shows that the amplitude of the horizontally polarized emission is linearly dependent on the magnetic field. The polarity of this induced voltage changes sign when the direction of the magnetic field flips direction, indicating that the transverse current flows in the opposite direction. The vertically polarized emission is observed to be constant with respect to magnetic field strength. The difference in slopes between the data and simulation is 20% which given our current systematic uncertainty should be taken as agreement between the two. This agreement along with the expectation that the ratio of magnetic emission to Askaryan emission scales with B/ρ confirms that transverse currents generate magnetic emission in air showers.

Several aspects of the radio emission in cosmic-ray air showers contribute to the formation of a conical beam pattern centered around the Cherenkov angle [32, 33]. In this experiment, the angular radiation pattern was measured by placing the antennas at different vertical positions. The power profile, which traverses the expected peak of the cone, is shown in Fig. 4 for three different frequency bands. Each profile is normalized by its total power.

The observed cones are somewhat different than those from air showers. In both cases, the expected power spectrum observed at the Cherenkov angle peaks at a frequency determined by the transverse size of the shower $L_\perp$, which is a fraction of a radiation length X_0. The Cherenkov cones have widths $\delta\theta = c/(nfL_\parallel \tan\theta_C)$, determined by the frequency of observation, f, the Cherenkov angle, θ_C, and the shower length, $L_\parallel$. At the peak power frequency, the width of the Cherenkov cone is determined simply by the aspect ratio of the shower $\delta\theta = L_\perp/L_\parallel$. For the T-510 beam of 4.5 GeV electrons, $L_\parallel \simeq 2X_0$ and we both predict and observe $\delta\theta \simeq 5°$. For air showers induced by 10^{17} eV primaries, $L_\parallel \simeq 5X_0$, and the inner edge of the Cherenkov cone is washed out because $\theta_C(1°) < \delta\theta(2°)$, causing the Cherenkov feature to appear as a filled-in disk, as observed by LOPES [34]. At higher frequencies, the width of the Cherenkov ring scales as $1/f$, and the ring becomes well defined, as observed at LOFAR [22] and inferred by ANITA [35]. The accurate simulation of the Cherenkov cone and frequency behavior shown in Fig. 4 is directly relevant to the ability of the simulations to model emission from air showers.

The signal polarization observed in T-510 confirms the paradigm that transverse currents due to the geomagnetic effect and longitudinal currents due to charge excess produce the radiation observed in air showers, consistent with measurements by CODALEMA [36] and AERA [21]. The observed Cherenkov cone in this work and at LOFAR [22] indicate that the refractive index is an important component to accurate modeling of the electrodynamics. Recent comparisons between the microscopic calculations and LOPES data confirm that first-principle calculations accurately predict the absolute scale of the radio emission [37], but the measurement is subject to uncertainties associated with air shower physics such as composition and hadronic interaction models. In using a fixed beam geometry and electromagnetic shower composition, this experiment confirms the absolute scale of the microscopic calculations with different systematic uncertainties.

We have presented the first laboratory benchmark of radio-frequency radiation from electromagnetic cascades under the influence of a magnetic field. We compared the radio emission produced in a well-defined target geometry with a well-defined particle shower to predictions made by microscopic models, which rely on first principles of electrodynamics and have no free parameters. The models agree and accurately predict the absolute scale of the radio emission to within our systematic uncertainty. The observed radiation grows linearly with magnetic field

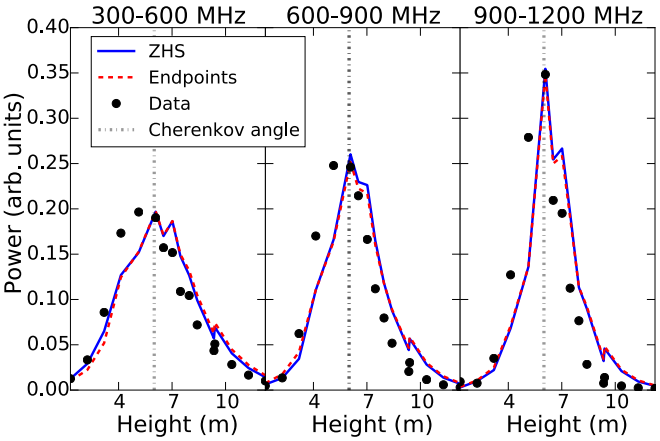

FIG. 4. Beam patterns for three frequency bands in the horizontal polarization at 970 G.

strength and forms a conical beam centered around the Cherenkov angle. Being in a relevant frequency range and independent of hadronic interaction models and complex geometries, this experiment is complementary to *in situ* observations of radio emission from air showers by current experiments [18, 20–22, 29, 35]. It also strengthens the case for proposed experiments based on the radio technique [38–41]. T-510 provides strong evidence that the electromagnetic simulations can be used to reliably predict the radio emission from extensive air showers.

We thank the referees and editors for critical remarks leading to an improved presentation. The authors thank SLAC National Accelerator Laboratory for providing facilities and support and especially Janice Nelson and Carl Hudspeth for their support and dedication that made T-510 possible. We thank D. Z. Besson for helpful discussions. This material is based upon work supported by the Department of Energy under Award Numbers DE-AC02-76SF00515, DE-SC0009937, and others. Work supported in part by grants from the National Aeronautics and Space Administration and the Taiwan Ministry of Science and Technology under project number MOST103-2119-M-002-002, among others. Part of this research was funded through the JPL Internal Research and Technology Development program. This work was supported in part by the Kavli Institute for Cosmological Physics at the University of Chicago through grant NSF PHY-1125897 and an endowment from the Kavli Foundation and its founder Fred Kavli. K. Belov acknowledges support from the Karlsruher Institut für Technologie under a guest fellowship. We are grateful to the ANITA collaboration for use of antennas and other equipment.

* Corresponding author: swissel@physics.ucla.edu, swissel@calpoly.edu

[1] G. A. Askaryan, JETP **14**, 441 (1962).
[2] D. Saltzberg *et al.*, Phys. Rev. Lett. **86**, 2802 (2001).
[3] P. W. Gorham *et al.*, Phys. Rev. E **62**, 8590 (2000).
[4] P. W. Gorham *et al.*, Phys. Rev. D **72**, 023002 (2005).
[5] P. W. Gorham *et al.*, Phys. Rev. Lett. **99**, 171101 (2007).
[6] P. Miočinović *et al.*, Phys. Rev. D **74**, 043002 (2006).
[7] J. V. Jelley *et al.*, Nature **205**, 327 (1965).
[8] N. A. Porter *et al.*, Physics Letters **19**, 415 (1965).
[9] S. N. Vernov *et al.*, JETP Letters **5**, 157, trans 126 (1967).
[10] P. R. Barker, W. E. Hazen, and A. Z. Hendel, Phys. Rev. Lett. **18**, 51 (1967).
[11] D. J. Fegan and P. J. Slevin, Nature **217**, 440 (1968).
[12] W. E. Hazen *et al.*, Phys. Rev. Lett. **22**, 35 (1969).
[13] W. E. Hazen *et al.*, Phys. Rev. Lett. **24**, 476 (1970).
[14] R. E. Spencer, Nature **222**, 460 (1969).
[15] D. J. Fegan and D. M. Jennings, Nature **223**, 722 (1969).
[16] H. R. Allan, *Progress in Elementary Particles and Cosmic Ray Physics*, edited by J. G. Wilson and S. G. Wouthuysen, Vol. 10 (North-Holland, Amsterdam, 1971) pp. 171–304, and references therein.
[17] H. Falcke *et al.*, Nature **435**, 313 (2005).
[18] D. Ardouin *et al.*, Astropart. Phys. **26**, 341 (2006).
[19] S. Hoover *et al.*, Phys. Rev. Lett. **105**, 151101 (2010).
[20] P. Schellart *et al.*, A&A **560**, A98 (2013).
[21] A. Aab *et al.*, Phys. Rev. D **89**, 052002 (2014).
[22] A. Nelles *et al.*, Astropart. Phys. **65**, 11 (2015).
[23] O. Scholten, K. Werner, and F. Rusydi, Astropart. Phys. **29**, 94 (2008).
[24] E. Zas, F. Halzen, and T. Stanev, Phys. Rev. D **45**, 362 (1992).
[25] C. W. James, H. Falcke, T. Huege, and M. Ludwig, Phys. Rev. E **84**, 056602 (2011).
[26] J. Alvarez-Muñiz, W. R. Carvalho, and E. Zas, Astropart. Phys. **35**, 325 (2012).
[27] T. Huege, M. Ludwig, and C. W. James, AIP Conf. Proc. **1535**, 128 (2013).
[28] J. Alvarez-Muñiz, A. Romero-Wolf, and E. Zas, Phys. Rev. D **81**, 123009 (2010).
[29] P. W. Gorham *et al.*, Astropart. Phys. **32**, 10 (2009).
[30] N. G. Lehtinen, P. W. Gorham, A. R. Jacobson, and R. A. Roussel-Dupre, Phys. Rev. D **69**, 013008 (2004).
[31] Krauss, J. D., *Antennas* (MacGraw-Hill, 1988).
[32] K. Belov *et al.*, AIP Conf. Proc. **1535**, 209 (2013).
[33] K. D. de Vries, A. M. van den Berg, O. Scholten, and K. Werner, Phys. Rev. Lett. **107**, 061101 (2011).
[34] W. D. Apel *et al.*, Phys. Rev. D **90**, 062001 (2014).
[35] H. Schoorlemmer *et al.*, Astropart. Phys. (2016), http://dx.doi.org/10.1016/j.astropartphys.2016.01.001.
[36] A. Bellétoile *et al.*, Astropart. Phys. **69**, 50 (2015).
[37] W. D. Apel *et al.*, Astropart. Phys. **75**, 72 (2016).
[38] P. W. Gorham *et al.*, Astropart. Phys. **35**, 242 (2011).
[39] A. Romero-Wolf *et al.*, arXiv:1302.1263 (2013).
[40] J. Nam *et al.*, Proc. of Science **ICRC2015**, 663 (2015).
[41] O. Martineau-Huynh *et al.*, Proc. of Science **ICRC2015**, 1143 (2015).